(α-$NaYbF_4$:Tm^{3+})/CaF_2 Core/Shell Nanoparticles with Efficient Near-Infrared to Near-Infrared Upconversion for High-Contrast Deep Tissue Bioimaging

Guanying Chen,[†,‡,⊥,◇] Jie Shen,[§,◇] Tymish Y. Ohulchanskyy,[‡] Nayan J. Patel,[∥] Artem Kutikov,[#] Zhipeng Li,[□] Jie Song,[#] Ravindra K. Pandey,[∥] Hans Ågren,[⊥] Paras N. Prasad,[†,‡,△,*] and Gang Han[§,*]

[†]School of Chemical Engineering and Technology, Harbin Institute of Technology, 150001 Harbin, People's Republic of China, [‡]Institute for Lasers, Photonics, and Biophotonics, University at Buffalo, State University of New York, Buffalo, New York 14260, United States, [⊥]Department of Theoretical Chemistry and Biology, Royal Institute of Technology, S-10691 Stockholm, Sweden, [§]Department of Biochemistry and Molecular Pharmacology, University of Massachusetts Medical School, Worcester, Massachusetts 01605, United States, [∥]Photodynamic Therapy Center, Roswell Park Cancer Institute, Buffalo, New York 14263, United States, [#]Department of Orthopedics and Department of Cell Biology, University of Massachusetts Medical School, Worcester, Massachusetts 01655, United States, [□]Department of Physics and Astronomy, University of North Carolina, Chapel Hill, North Carolina 27599, United States, and [△]Department of Chemistry, Korea University, Seoul, Korea, 136-701. [◇]Equal contributions.

ABSTRACT

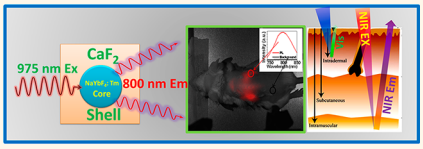

We describe the development of novel and biocompatible core/shell (α-$NaYbF_4$:Tm^{3+})/CaF_2 nanoparticles that exhibit highly efficient NIR_{in}—NIR_{out} upconversion (UC) for high contrast and deep bioimaging. When excited at ~980 nm, these nanoparticles emit photoluminescence (PL) peaked at ~800 nm. The quantum yield of this UC PL under low power density excitation (~0.3 W/cm^2) is 0.6 ± 0.1%. This high UC PL efficiency is realized by suppressing surface quenching effects *via* heteroepitaxial growth of a biocompatible CaF_2 shell, which results in a 35-fold increase in the intensity of UC PL from the core. Small-animal whole-body UC PL imaging with exceptional contrast (signal-to-background ratio of 310) is shown using BALB/c mice intravenously injected with aqueously dispersed nanoparticles (700 pmol/kg). High-contrast UC PL imaging of deep tissues is also demonstrated, using a nanoparticle-loaded synthetic fibrous mesh wrapped around rat femoral bone and a cuvette with nanoparticle aqueous dispersion covered with a 3.2 cm thick animal tissue (pork).

KEYWORDS: near-infrared · photoluminescence bioimaging · upconversion nanocrystals · lanthanide · core/shell

Optical imaging plays an important role in biomedical research, being extremely useful for early detection, screening, and image-guided therapy of life-threatening diseases. Photoluminescence (PL) optical imaging excels in bioimaging applications due to fast and robust imaging, high resolution and sensitivity, and low biological toxicity.[1,2] However, PL imaging of deep tissue has been significantly hindered because of insufficient tissue light transmission and high scattering. PL probes for deep tissue *in vivo* imaging should have the following properties: (1) nontoxicity; (2) both the excitation light and PL emission being in the spectral range favorable for penetration of light through thick tissues due to minimal light scattering and tissue autofluorescence, and (3) efficient and stable PL signal. PL imaging commonly employs Stokes-shifted probes, such as organic fluorophores, semiconductor quantum dots, and quantum rods, which absorb and produce emission in the visible range.[3−5] In spite of their overall high PL efficiency, the *in vivo* PL imaging quality and depth obtained with these contrast agents are limited due to low tissue penetration in the visible range and often a strong background from autofluorescence and light scattering. Although the signal-to-background ratio (SBR) can be enhanced by the application of complex spectral unmixing algorithms, which separate the PL and the background signals, the imaging depth cannot be improved in this process.[6] Since endogenous fluorophores in tissue generally manifest Stokes fluorescence in conventional optical imaging, nanoprobes with anti-Stokes PL are preferable, as there is zero autofluorescence in the detection channel. Another factor impeding the biomedical application of current PL imaging probes is the poor photostability of organic

* Address correspondence to pnprasad@buffalo.edu, gang.han@umassmed.edu.

Received for review July 3, 2012 and accepted August 28, 2012.

Published online August 28, 2012
10.1021/nn302972r

dyes[3] and potential toxicity of quantum dots and quantum rods that contain toxic elements (*e.g.*, cadmium, selenium, and lead).[7] Although nontoxic, one-photon-excitable Stokes PL nanoprobes with excitation and emission in the near-infrared (NIR) range are being investigated to allow high penetration in tissues, their success remains limited due to a lack of highly bright, stable, and biocompatible Stokes emitters.[8−10] To eliminate strong autofluorescence and the light-scattering background resulting from excitation with ultraviolet or visible light and to improve SBR and imaging depth, nanomaterials converting light from NIR to visible (*e.g.*, two-photon-excited quantum rods,[11] gold nanorods,[12] and second-harmonic-generation active nanoparticles[13]) have been proposed. Although a high SBR was achieved with these nanoprobes for cellular imaging *in vitro*, it remains problematic for high-contrast *in vivo* bioimaging because of low efficiency of light upconversion and the need for an expensive laser to provide the required excitation power density of $\sim 10^6-10^9$ W/cm^2.[2,14,15] Another challenge of using nonlinear nanoprobes for deep tissue optical imaging is the high scattering of biological tissue in the visible range.[1] A utilization of the "optical transmission window" for biological tissues in the NIR range ($\sim$700−1000 nm)[2] for both excitation and emission not only allows a deep light penetration and reduced photodamage but also produces low autofluorescence and light scattering. Hence, the development of efficient and biocompatible anti-Stokes nanoprobes with excitation and PL within the NIR window of tissue optical transmission is of great interest for high-contrast optical imaging of deep tissues.

An attractive alternative to two-photon-excitable nanomaterials for bioimaging applications is lanthanide-doped upconverting nanoparticles (UCNPs).[16−20] Upconversion (UC) in lanthanide ions is a process that converts the excitation light with a longer wavelength (*e.g.*, NIR) into emission at a shorter wavelength in ultraviolet, visible, or NIR, using a ladder-like system of energy levels of lanthanide ions.[21−23] This process involves a stepwise photon mechanism and is orders of magnitude more efficient than the conventional, simultaneous multiphoton absorption process,[23] allowing excitation with low-cost continuous-wave laser diodes at a relatively low-energy excitation density of $10^{-1}-10^2$ W/cm^2. Lanthanide-doped UCNPs have demonstrated high photostability and low toxicity, making them suitable candidates for *in vitro* and *in vivo* optical imaging applications.[24−26] Despite recent successes in UC PL bioimaging,[19] *in vivo* imaging with high SBR and deep-tissue penetration capability has not been conclusively established due to the low efficiency of existing UCNPs. The highest quantum yields (QY) reported to date for upconverting PL are $\sim$1.2% for 85 nm tetragonal $LiYF_4:Er^{3+}$ nanocrystals[27] under 1490 nm excitation with a power density of 10−150 W/cm^2 and $\sim$3.5% for 45 nm hexagonal ($NaYF_4:Yb^{3+}/Tm^{3+}$)/$NaYF_4$ core/shell nanocrystals excited at 980 nm with a power density of $\sim$78 W/cm^2.[28] As the generation of UC PL involves multiphoton processes, the QY of UC PL will be dependent on the excitation power density (*e.g.*, the linear dependence for two-photon-induced UC PL). Therefore, when the excitation density is decreased to the level of $\sim 10^{-1}$ W/cm^2, which is used for optical imaging *in vivo*, the QY of UC PL becomes hundreds of times lower than those reported.[27−29] For example, the QY of UC PL from 45 nm hexagonal ($NaYF_4:Yb^{3+}/Tm^{3+}$)/$NaYF_4$ core/shell NPs is 0.038% when excited at a lower energy of 0.22 W/cm^2; this quantum yield is 92 times lower than that measured at $\sim$78 W/cm^2.[28] Although weak UC PL (even a single photon) was reported to be detected by an expensive but highly sensitive electron-multiplied charge-coupled devices (EMCCD),[30] it is highly desirable to construct UC PL nanoprobes, both excited and emitting in the NIR range ($NIR_{in}-NIR_{out}$), which would be efficient enough under low power of excitation to be detected and imaged by commercial imaging CCDs for high-contrast bioimaging of deep tissues.

We first reported high-contrast *in vitro* and *in vivo* bioimaging using $NIR_{in}-NIR_{out}$ UC PL nanocrystals ($NaYF_4:Yb^{3+}/Tm^{3+}$), where excitation at $\sim$980 nm and the PL peak at 800 nm are both within the NIR optical transmission window of biological tissues.[31] Since then, $NIR_{in}-NIR_{out}$ UCNPs are being developed as promising bioimaging probes, allowing low imaging background with deep tissue penetration,[19] but their low efficiency, even with EMCCD detection, is still a substantial limitation for improving the SBR and the imaging depth. Various methods have been proposed to improve the UCNPs' efficiency.[32−36] We have recently established a novel strategy that not only results in an 8-fold enhancement of the quantum yield of NIR UC PL but also increases the extinction coefficient of every nanoparticle 5 times by elevating the concentration of the sensitizer (Yb^{3+}).[36] In this paper, we demonstrate that the PL of the previously designed[36] $NIR_{in}-NIR_{out}$ α-$NaYbF_4:Tm^{3+}$ UCNPs is enhanced 35 times by encapsulating them in a heteroshell of CaF_2, which efficiently suppresses surface quenching, yielding a QY as high as 0.6 ± 0.1% under excitation with a low power density of $\sim$0.3 W/cm^2. CaF_2 was chosen as the epitaxial shell material due to its low lattice mismatch with α-$NaYbF_4$, good optical transparency, high crystallizability, and stability.[37−39] Furthermore, the CaF_2 shell enhances the biocompatibility of UCNPs, as calcium and fluoride ions are common endogenous components and lattice substituents of calcified tissues (*i.e.*, bone and teeth). Using an aqueous dispersion of these efficient $NIR_{in}-NIR_{out}$ $NaYbF_4:Tm^{3+}/CaF_2$ core/shell nanoparticles, intravenously injected in BALB/c mice, we have performed UC PL whole-body imaging; a high SBR of 310 has been achieved. We have

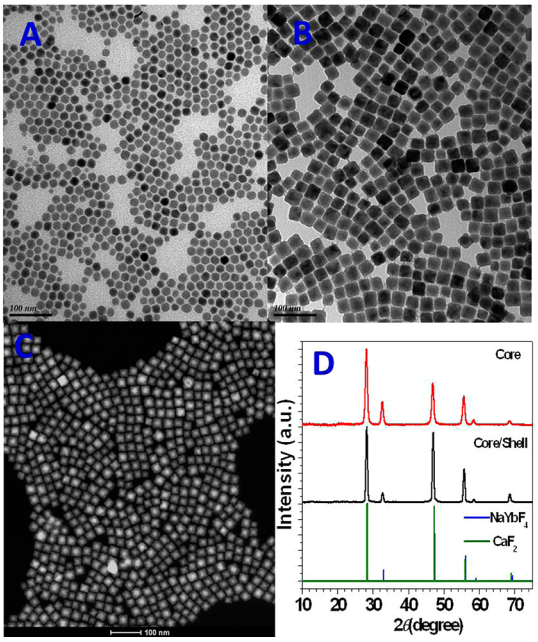

Figure 1. Successful epitaxial growth of CaF_2 shells on $NaYbF_4$:0.5% Tm^{3+} core nanoparticles, resulting in uniform and monodispersed ($NaYbF_4$:0.5% Tm^{3+})/CaF_2 core/shell nanoparticles. Transmission electron microscopy images of (a) $NaYbF_4$:0.5% Tm^{3+} core and (b) ($NaYbF_4$:0.5% Tm^{3+})/CaF_2 core/shell nanoparticles. (c) High-angle annular dark-field scanning transmission electron microscopy image of ($NaYbF_4$:0.5% Tm^{3+})/CaF_2 nanoparticles with resolved core/shell structures; both the core (bright) and the shell (dark) are clearly visible. (d) Powder X-ray diffraction patterns of $NaYbF_4$:0.5% Tm^{3+} core and ($NaYbF_4$:0.5% Tm^{3+})/CaF_2 core/shell particles.

also shown that the UC PL signal can be readily detected and imaged, with a low background, through a 3.2 cm thick pork tissue and from a synthetic fibrous mesh wrapped around a rat femoral bone.

RESULTS AND DISCUSSION

Synthesis and Characterizations of Core/Shell ($NaYbF_4$:0.5% Tm^{3+})/CaF_2 Nanocrystals with Efficient NIR-to-NIR Upconversion Photoluminescence. The synthesized $NaYbF_4$:0.5% Tm^{3+} core nanoparticles were monodispersed nanopolyhedra with an average diameter of about 20 nm (Figure 1a). After growing a CaF_2 shell, the resulting ($NaYbF_4$:0.5% Tm^{3+})/CaF_2 core/shell nanoparticles were monodispersed nanocubes, with an average size of about 27 nm (Figure 1b). The core/shell structure is clearly seen in high-angle annular dark-field (HAADF) scanning transmission electron microscopy (STEM), which is highly sensitive to variations in the atomic number of atoms in the sample (Z-contrast images) (Figure 1c). The energy-dispersive X-ray spectroscopic (EDX) line scan conducted with STEM imaging on a ($NaYbF_4$:0.5% Tm^{3+})/CaF_2 nanoparticle indicated a higher Ca concentration in the peripheral region and a higher Yb concentration in the center region of the crystal that is highly consistent with the designed core−shell structure (see Supporting Information, Figure S1). The powder X-ray diffraction peaks of the $NaYbF_4$:0.5% Tm^{3+} core and the ($NaYbF_4$:0.5% Tm^{3+})/CaF_2 core/shell nanoparticles in Figure 1d have identical positions to the standard JCPDS 06-0258 cubic $NaYbF_4$ (α-$NaYbF_4$) or JCPDS 77-2095 cubic CaF_2 (α-CaF_2) structures. In addition, the peak intensity at 47° is relatively higher for the core/shell nanoparticles than that for the core nanoparticles, which corresponds to the difference between the standard JCPDS 06-0258 α-$NaYbF_4$ and JCPDS 77-2095 CaF_2 structures. This observation indicates a successful epitaxial growth of CaF_2 shells on the α-$NaYbF_4$:0.5% Tm^{3+} core nanoparticles, along with the HAADF STEM image shown in Figure 1c.

The UC PL spectra of the α-$NaYbF_4$:0.5% Tm^{3+} core and the α-($NaYbF_4$:0.5% Tm^{3+})/CaF_2 core/shell nanoparticles dispersed in hexane are shown in Figure 2a. For a comparison of the UC PL efficiency from the core and the core/shell nanoparticles, the absorption spectra were normalized at the excitation wavelength (975 nm) for the $^2F_{7/2} \rightarrow {}^2F_{5/2}$ transition of Yb^{3+} ions, by adjusting the concentration (Figure 2a, inset). Four UC PL bands can be clearly resolved; they have maxima at 476, 650, 700, and 802 nm, corresponding to the $^1G_4 \rightarrow {}^3H_6$, $^1G_4 \rightarrow {}^3F_4$, $^3F_{2,3} \rightarrow {}^3H_6$, and $^3H_4 \rightarrow {}^3H_6$ transitions of the Tm^{3+} ions, respectively.[40] The NIR UC PL peak at 802 nm, representing a sequential two-photon process,[36] is the most intense, favoring bioimaging applications. The intensity of NIR UC PL from the core/shell nanoparticles is about 35 times higher than that from the core-alone nanoparticles. This difference in intensity is also illustrated by the photographic images of cuvettes with suspensions of the core and the core/shell nanoparticles under laser excitation at 975 nm (Figure 2b), where the visible blue emission (peaked at 476 nm) from the core/shell nanoparticles is much brighter than that from the core-alone nanoparticles. The higher intensity of UC PL from the core/shell nanoparticles undoubtedly originates from the effect of the shell on the core α-$NaYbF_4$:Tm^{3+}0.5% nanocrystals; UC PL surface quenching is suppressed due to decreased surface defects and alleviation of the ligand influence by the shell layer. This is confirmed by the measurements of the decays of UC PL (peaked at 802 nm) from the core and the core/shell nanoparticles (Figure 2c). The average PL lifetime for the core/shell nanoparticles is 300 μs, significantly longer than the 90 μs lifetime of the core nanoparticles, demonstrating that the enhancement of UC PL arises from efficient suppression of surface-quenching effects.[40,41] Hexagonal crystalline structure and larger size are factors known to facilitate higher efficiency for the UCPL from lanthanide-doped nanocrystals. For example, visible UC PL in β-$NaYF_4$:Yb^{3+}/Er^{3+} material is 4.4 times more intense than in the α-$NaYF_4$:Yb^{3+}/Er^{3+} material,[42] and the QY of UC PL from the 100 nm β-$NaYF_4$:Yb^{3+}/Er^{3+} nanoparticles is 3 times higher than that of the 30 nm

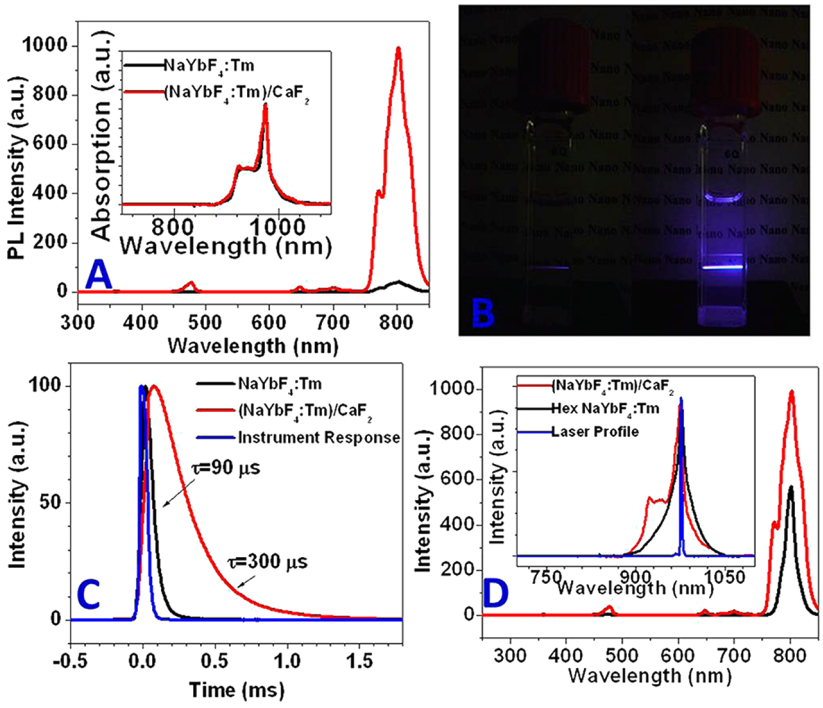

Figure 2. Optical characterizations of ($NaYbF_4$:0.5% Tm^{3+})/CaF_2 core/shell UCNPs (hexane suspensions). (a) Upconversion photoluminescence spectrum under laser excitation at 975 nm, (b) photographic images of cuvettes with suspensions of the core and the core/shell nanoparticles under laser excitation at 975 nm, (c) decays of PL at 802 nm for the α-$NaYbF_4$:0.5% Tm^{3+} core and the α-($NaYbF_4$:0.5% Tm^{3+})/CaF_2 core/shell nanoparticles, and (d) upconversion PL spectra of 27 nm α-($NaYbF_4$:0.5% Tm^{3+})/CaF_2 core/shell nanoparticles and 100 nm β-$NaYbF_4$:0.5% Tm^{3+} (hexagonal) nanoparticles when excited by a 975 nm CW diode laser at a power density of ~0.3 W/cm^2. The insets in (a) and (d) show the absorption spectra of UCNPs (normalized at the PL excitation wavelength for the $^2F_{7/2} \rightarrow {}^2F_{5/2}$ transition of Yb^{3+} ions).

β-$NaYF_4$:Yb^{3+}/Er^{3+} nanoparticles.[43] Comparison of the emission spectra of the synthesized core/shell nanoparticles with those of larger β-$NaYbF_4$:0.5% Tm^{3+} nanoparticles shows that the integrated NIR UC PL intensity of the 27 nm α-($NaYbF_4$:0.5% Tm^{3+})/CaF_2 core/shell nanoparticles is about 2 times higher than that of 100 nm β-$NaYbF_4$:0.5% Tm^{3+} nanoparticles (Figure 2d), demonstrating high efficiency of the core/shell nanoparticles. The quantum yield of NIR UC PL in the 27 nm α-($NaYbF_4$:0.5% Tm^{3+})/CaF_2 core/shell nanoparticles was measured to be 0.60 ± 0.1% under low-energy excitation of 0.3 W/cm^2, using IR 26 as a standard reference (see Supporting Information). Considering that this high QY for NIR UC PL was obtained with low-energy excitation density, we envisage that the α-($NaYbF_4$:0.5% Tm^{3+})/CaF_2 core/shell nanoparticles are promising nanoprobes for bioimaging applications.

High Contrast *in Vitro* Bioimaging Using Water-Dispersed Core/Shell α-($NaYbF_4$:0.5% Tm^{3+})/CaF_2 Nanocrystals. To verify the feasibility of cellular imaging using the NIR_{in}–NIR_{out} α-($NaYbF_4$:0.5% Tm^{3+})/CaF_2 core/shell nanoparticles as UC PL imaging probes, we transferred the nanoparticles to an aqueous phase by coating them with hyaluronic acid (HA, an anionic, nonsulfated glycosaminoglycan) and treated the cultured living cells (HeLa) with the HA-coated nanoparticles. After incubation with the nanoparticles for 2 h, cells were imaged using a Nikon Eclipse TE 2000 microscope, equipped with a Nuance CCD camera (Cambridge Research & Instrumentation Inc., CRi) capable of imaging in the spectral range 500–950 nm. The light source was a fiber-coupled laser diode emitting at ~980 nm, with the fiber introduced through the entrance port of the microscope.[31] Figure 3 shows the transmission and the PL images of the HeLa cells treated with UCNPs after excitation at 980 nm. The localized emission spectrum from the cells shows the characteristic Tm^{3+} PL peak at ~800 nm (Figure 3, right, inset). A complete absence of autofluorescence in the imaging wavelength range 500–950 nm supports that UCNPs are uniquely suited for high-contrast PL imaging of the living cells *in vitro*.

High Contrast *in Vivo* Bioimaging Using Water-Dispersed Core/Shell α-($NaYbF_4$:0.5% Tm^{3+})/CaF_2 Nanocrystals. To examine the suitability of the α-($NaYbF_4$:0.5% Tm^{3+})/CaF_2 core/shell nanoparticles for *in vivo* imaging, we injected a BALB/c mouse intravenously (*via* tail vein) with the HA-coated core/shell nanoparticles (700 pmol/kg). The hair on the back of the mouse was shaved, while the hair on the belly remained unshaved. The BALB/c mouse was imaged for *in vivo* PL at 3 h postinjection using the Maestro fluorescence imaging system (CRi), as described previously.[31] The core/shell nanoparticles were excited at 980 nm by the fiber-coupled laser diode introduced into the imaging chamber; the laser beam diverged from the fiber end. The scattered

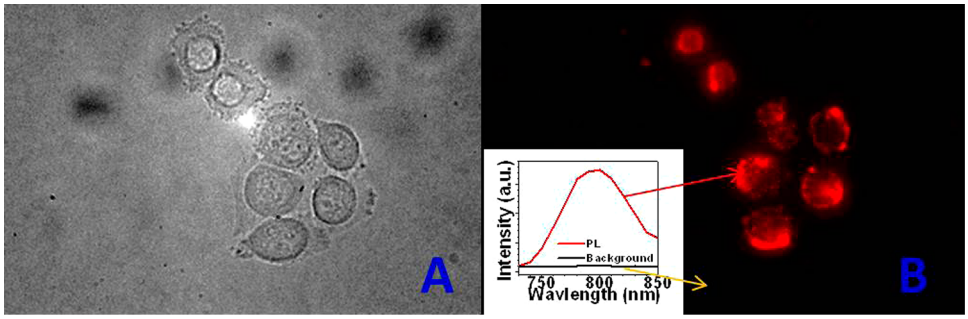

Figure 3. *In vitro* **transmission (a) and UCPL (b) images of HeLa cells treated with α-($NaYbF_4$:0.5% Tm^{3+})/CaF_2 core/shell nanoparticles coated with hyaluronic acid (HA).**

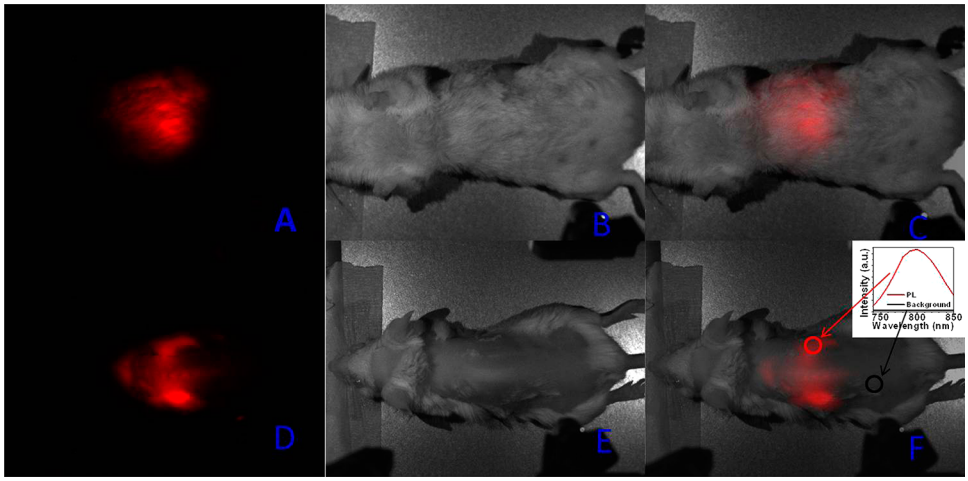

Figure 4. Whole-animal imaging of a BALB/c mouse injected *via* tail vein with the HA-coated α-($NaYbF_4$:0.5% Tm^{3+})/CaF_2 core/shell nanoparticles. (a, d) UC PL images; (b, e) bright-field images; and (c, d) merged bright-field and UC PL images. Mouse was imaged in the belly (a, b, c) and the back positions. Inset in (f) shows the spectra of the NIR UC PL and background taken from the circled area.

excitation light was cut off by an emission filter (850 SP, Andover) in front of the imaging camera objective. A high-contrast image of the mouse injected with the core/shell nanoparticles (Figure 4) demonstrates that it is feasible to image and spectrally distinguish the characteristic emission of the nanoparticles using the Maestro imaging system. An intense PL was clearly seen, with the peak at ~800 nm (shown in red in Figure 4f). The UCPL signal was readily detectable through the skin of shaved and unshaved parts of the mouse. The SBR, defined by the ratio of the integrated PL intensity in the area of interest (red circle) to that in the same area of surrounding tissues (black circle), is 310, about 10-fold greater than that reported for *in vivo* imaging by UCNPs.[30] The high contrast between the background and the PL signal of UCNPs results from efficient UC PL from the core/shell nanoparticles. It is important to note that no overt toxicity was observed in the mouse injected with the HA-coated core/shell nanoparticle; they remained visibly healthy during eight months postinjection. Furthermore, after sacrificing the mouse injected with the HA-coated core/shell nanoparticles, their main organs were extracted and examined in the Maestro system; no UCPL signal was found (data not shown). This may suggest that eight months postinjection the presence of nanoparticles in the body decreased to a nondetectable level due to excretion.

High Contrast Imaging-Guided Tissue Engineering and Deep Tissue Bioimaging Using Core/Shell α-($NaYbF_4$:0.5% Tm^{3+})/CaF_2 Nanocrystals. We have studied the tissue penetration depth and the possibility for imaging of a polymer fibrous mesh implanted around rat femoral bone as potential synthetic periosteal membrane with preabsorbed α-($NaYbF_4$:0.5% Tm^{3+})/CaF_2 core/shell nanoparticles for image-guided tissue-engineering applications. The polyethyleneimine-coated NIR_{in}—NIR_{out} α-($NaYbF_4$:0.5%Tm^{3+})/CaF_2 core/shell nanoparticles were absorbed on a sulfated polymeric fibrous mesh, which was then wrapped around a rat femur, as shown in Figure 5a. The sulfated mesh was chemically modified from thermal-mechanically annealed electrospun cellulose acetate fibrous mesh.[44] The sulfated mesh (7 mm × 10 mm × 0.1 mm) was loaded with 4 μg of the core/shell particles (400 μL of 10 μg/mL aqueous suspension) by repeated loading/drying (in vacuum oven; rt). The hind leg of a freshly sacrificed adult male Sprague—Dawley rat (441 g) was shaved, and its

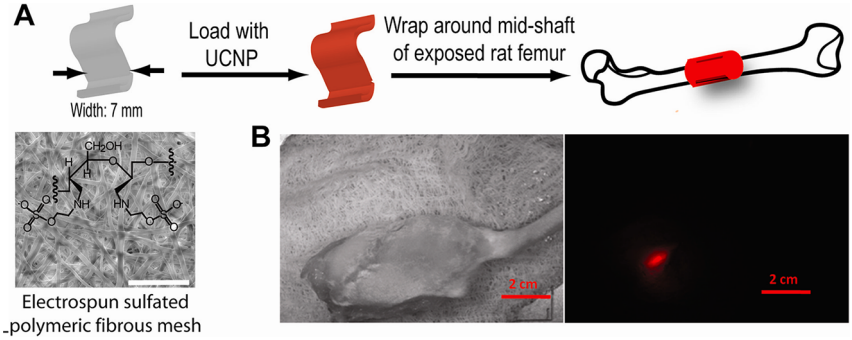

Figure 5. Polyethyleneimine-coated NIR_{in}—NIR_{out} α-($NaYbF_4$:0.5%Tm^{3+})/CaF_2 core/shell nanoparticles for imaging a synthetic periosteal mesh implanted around a rat femur. (a) UCNPs were loaded on a 7 mm wide sulfated polymer mesh and wrapped around the midshaft of a rat femur. Scale bar: 500 μm. (b) Bright-field image of the rat hind leg after closing muscle/skin by suture (left) and PL image (right) of the deeply embedded UCNP-stained synthetic mesh wrapped around the rat femur. Scale bar: 2 cm.

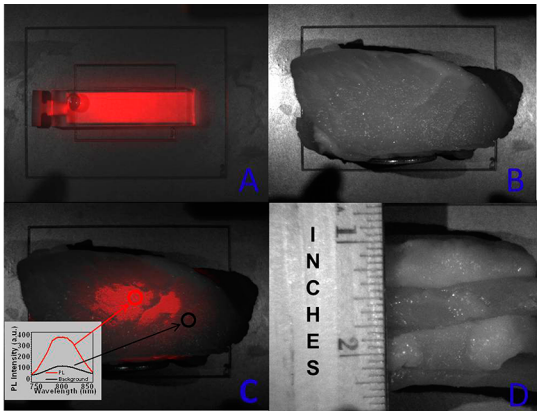

Figure 6. (a) UCPL bright-field image of a cuvette filled with a suspension of the core/shell nanoparticles, (b) bright-field image of a cuvette covered with pork tissue with a quarter coin stood aside showing its thickness, (c) merged UCPL/bright-field image of the cuvette covered with pork tissue, and (d) bright-field image of the pork tissue (side view). The inset in (c) shows the spectra obtained from the circled areas.

femoral bone (outer diameter ~4 mm) was exposed by a combination of sharp and blunt dissections. The periosteal tissue, attached to the exposed femur, was removed by a bone elevator, and the UCNP-loaded synthetic mesh was circumferentially wrapped around the exposed femur. The muscle and tissue were then suture-closed in layers (3.0 chromic gut suture). The thickness of the operated hind leg, including the femoral bone and surrounding muscle, was approximately 16 mm. Seven days after the UCNP-loaded mesh was implanted, the operated hind leg was imaged (Figure 5). A vibrant UC PL image of the UCNP-loaded mesh can be readily visualized around the femur against the background, suggesting that these UCNPs can be employed for image-guided tissue engineering applications.

Finally, to explore the possibility of imaging of UCPL from a deeper tissue, we placed a 1.25 inch (3.2 cm) slice of pork tissue on top of a cuvette filled with a suspension of the α-($NaYbF_4$:0.5% Tm^{3+})/CaF_2 UCNPs core/shell nanoparticles (225 nM) and imaged it with the Maestro system. The NIR upconverted emission can be clearly distinguished from the light-scattering background, with a SBR of about 3 (Figure 6). This imaging depth, demonstrated for the NIR_{in}—NIR_{out} UCNPs, would be of great use for *in vivo* imaging.

CONCLUSIONS

In conclusion, we report novel core/shell α-($NaYbF_4$:0.5% Tm^{3+})/CaF_2 nanoparticles with efficient NIR_{in}—NIR_{out} UC PL and their applications for high-contrast *in vitro* and deep tissue bioimaging. An epitaxial CaF_2 heteroshell increases the intensity of UC PL from α-$NaYbF_4$:0.5% Tm^{3+} nanoparticles 35 times; the quantum yield of the increased UC PL is 0.6 ± 0.1% under low-energy excitation of 0.3 W/cm^2. Furthermore, whole-body imaging of a BALB/c mouse intravenously injected with an aqueous dispersion of the core/shell nanoparticles (700 pmol/kg) showed a SBR of 310, about 10-fold higher than that previously reported for *in vivo* imaging by UCNPs. The retention of the NIR_{in}—NIR_{out} ($NaYbF_4$:Tm^{3+})/CaF_2 nanoparticles on a synthetic scaffold surrounding a rat femoral bone under centimeter-deep soft tissues was successfully visualized, demonstrating the potential of these nanoparticles for image-guided tissue engineering applications. Finally, UC PL from a ($NaYbF_4$:Tm^{3+})/CaF_2 nanoparticle suspension was imaged through 3.2 cm pork tissue, with a high contrast against the background. The observed capabilities of our engineered NIR_{in}—NIR_{out} upconversion nanoparticles provide promise for their wide application in biomedical imaging.

METHODS

Synthesis of Core/Shell α-($NaYbF_4$:0.5% Tm^{3+})@CaF_2 Upconversion Nanoparticles. All chemicals used in the synthesis were purchased from Sigma-Aldrich and used as received. A mixture of oleic acid (8 mmol) and 1-octadecene (8 mmol) was heated to 120 °C in a three-neck flask for vacuum degassing. It was then heated to

310 °C under argon protection. A precursor solution of α-$NaLnF_4$ core was prepared by mixing CF_3COONa (0.5 mmol) and $Ln(CF_3COO)_3$ (Ln = Y, Yb, Tm, 0.5 mmol in total) with oleic acid (5 mmol) and 1-octadecene (5 mmol). After removing trace oxygen and water, this precursor solution was injected into the flask at a rate of *ca.* 1 mL/min. The reaction mixture was kept at 310 °C for 1 h under dry argon. Then, a degassed oleic acid (5 mmol)/1-octadecene (5 mmol) solution with $Ca(CF_3COO)_2$ (2 mmol) was injected at the same rate. The reaction was continued for 1 h more at 310 °C. The α-$NaLnF_4$@CaF_2 UCNPs were precipitated by adding ethanol to the cooled reaction flask. After centrifugal washing with hexane/ethanol, the resulting white powder was redispersed into 20 mL of toluene for the following ligand exchange procedure. The core α-$NaLnF_4$ UCNPs could be obtained by removing the heating source after the first 1 h of reaction.

Water-Soluble Core/Shell α-($NaYbF_4$:0.5% Tm^{3+})@CaF_2 Upconversion Nanoparticles by Ligand Exchange. The ligand exchange was performed following a literature method.[45] Poly(acrylic acid) (PAA, M_w 1800, 0.500 g) in diethylene glycol (8.0 mL) was heated to 110 °C, with vigorous stirring under argon flow. A 2 mL amount of a toluene solution of UCNPs (0.03 g) was then injected, and the mixture was heated to reflux for 1 h (*ca.* 240 °C) to remove toluene. After cooling the solution, excess deionized water was added and water-soluble UCNPs were collected by centrifugal precipitation. The UCNPs were further purified in DI water three times by high-speed centrifugation and preserved in 5 mL of DI water for further modification.

HA-Coated Core/Shell α-($NaYbF_4$:0.5% Tm^{3+})@CaF_2 Upconversion Nanoparticles Using the Layer-by-Layer (LbL) Technique. UCNPs coated with a functional polymer were prepared by a commonly used assembly technique for nanoparticles.[46] Branched polyethylenimine (PEI, M_w ~25 000, Aldrich) and sodium hyaluronate (M_w ~10 000, Lifecore Biomedical Inc.) were dissolved in DI water to prepare stock solutions at a concentration of 10 mg/mL, respectively. The pH value was adjusted to 7.4 by adding diluted hydrochloric acid. For LbL assembly, the PAA-coated UCNP solution was mixed vigorously with the same volume of PEI solution. After 4 h of reaction, the PEI-coated UCNPs were purified by three centrifugal washings. Using a similar method, the PEI-coated UCNPs were further assembled with HA to obtain HA-coated UCNPs.

Characterizations of Core α-($NaYbF_4$:0.5% Tm^{3+}) and Core/Shell α-($NaYbF_4$:0.5% Tm^{3+})@CaF_2 Upconversion Nanoparticles. The size and the morphology of the core and core/shell nanocrystals were characterized by transmission electron microscopy (TEM) using a JEM-2010 microscope at an acceleration voltage of 200 kV. The core/shell structure is resolved by a HAADF scanning transmission electron microscopy using a JEOL 2010 F microscope operating at 200 kV. The 2D elemental mapping of the core/shell nanoparticle is recorded by an energy-dispersive X-ray spectroscopy (EDX) detector in the JEOL 2010 F STEM microscope. The powder X-ray diffraction (XRD) patterns were recorded by a Siemens D500 diffractometer using Cu Kα radiation (λ = 0.15418 nm). The 2θ angle of the XRD spectra was recorded at a scanning rate of 5°/min. Absorption spectra of transparent colloidal nanocrystals were acquired using a Shimadzu UV−visible−NIR scanning spectrophotometer. UC photoluminescence spectra were recorded using a Fluorolog-3.11 Jobin Yvon spectrofluorimeter with a slit width defining a spectral resolution of 1 nm. The PL was excited at 975 nm using a fiber-coupled laser diode (Q-Photonics) introduced to the sample chamber of the spectrofluorimeter. All UC PL spectra have been corrected for the spectral sensitivity of the system. Photographic images of UC colloidal nanocrystals were taken by a digital camera (Lumix DMC-Fx520, Japan) without adding any filter. The PL decays at 802 nm were acquired using an Infinium oscilloscope (Hewlett-Packard) coupled to the PMT of a Fluorolog-3.11 Jobin Yvon spectrofluorometer. When measuring the PL decays, the laser diode was operated in a pulsed mode with a repetition of 200 Hz and a pulse width of 50 μs.

Conflict of Interest: The authors declare no competing financial interest.

Acknowledgment. This work was supported in part by grants from the National Institutes of Health (R01CA119358 and RO1CA104492), the Swedish Energy Agency (project 32076-1), Natural Science Foundation of China (51102066), the John R. Oishei Foundation, and the Start-up Funding from University of Massachusetts−Medical School.

Supporting Information Available: EDX elemental mapping of a core/shell nanoparticle; details of determination of quantum yield for NIR UC PL, and calculation of "molecular weight" of core/shell α-($NaYbF_4$:0.5% Tm^{3+})@CaF_2 UCNPs. This material is available free of charge *via* the Internet at http://pubs.acs.org.

REFERENCES AND NOTES

1. Prasad, P. N. *Introduction to Biophotonics*; Wiley-Interscience: New York, 2003; pp 255−360.
2. Prasad, P. N. *Introduction to Nanomedicine and Nanobioengineering*; Wiley-Interscience: NJ, 2012; pp 171−180.
3. Hilderbrand, S. A.; Weissleder, R. Near-Infrared Fluorescence: Application to *in Vivo* Molecular Imaging. *Curr. Opin. Chem. Biol.* **2010**, *14*, 71–79.
4. Smith, A. M.; Mancini, M. C.; Nie, S. M. Second Window for *in Vivo* Imaging. *Nat. Nanotechnol.* **2009**, *4*, 710–711.
5. Alivisatos, P. The Use of Nanocrystals in Biological Detection. *Nat. Biotechnol.* **2004**, *22*, 47–52.
6. Farkas, D. L.; Du, C. W.; Fisher, G. W.; Lau, C.; Niu, W. H.; Wachman, E. S.; Levenson, R. M. Non-linvasive Iimage Acquisition and Advanced Processing in Optical Bioimaging. *Comput. Med. Imaging Graphics* **1998**, *22*, 89–102.
7. Sharrna, P.; Brown, S.; Walter, G.; Santra, S.; Moudgil, B. Nanoparticles for Bioimaging. *Adv. Colloid Interface Sci.* **2006**, *123*, 471–485.
8. Welsher, K.; Liu, Z.; Sherlock, S. P.; Robinson, J. T.; Chen, Z.; Daranciang, D.; Dai, H. J. A Route to Brightly Fluorescent Carbon Nanotubes for Near-Infrared Imaging in Mice. *Nat. Nanotechnol.* **2009**, *4*, 773–780.
9. Gao, J. H.; Chen, K.; Xie, R. G.; Xie, J.; Lee, S.; Cheng, Z.; Peng, X. G.; Chen, X. Y. Ultrasmall Near-Infrared Non-cadmium Quantum Dots for *in Vivo* Tumor Imaging. *Small* **2010**, *6*, 256–261.
10. Chen, G. Y.; Ohulchanskyy, T. Y.; Liu, S.; Law, W. C.; Wu, F.; Swihart, M. T.; Ågren, H.; Prasad, P. N. Core/Shell $NaGdF_4$:Nd^{3+}/$NaGdF_4$ Nanocrystals with Efficient Near-Infrared to Near-Infrared Downconversion Photoluminescence for Bioimaging Applications. *ACS Nano* **2012**, *6*, 2969–2977.
11. Yong, K. T.; Qian, J.; Roy, I.; Lee, H. H.; Bergey, E. J.; Tramposch, K. M.; He, S. L.; Swihart, M. T.; Maitra, A.; Prasad, P. N. Quantum Rod Bioconjugates as Targeted Probes for Confocal and Two-Photon Fluorescence Imaging of Cancer Cells. *Nano Lett.* **2007**, *7*, 761–765.
12. Wang, H. F.; Huff, T. B.; Zweifel, D. A.; He, W.; Low, P. S.; Wei, A.; Cheng, J. X. *In Vitro* and *in Vivo* Two-Photon Luminescence Imaging of Single Gold Nanorods. *Procl. Natl. Acad. Sci. U. S. A.* **2005**, *102*, 15752–15756.
13. Kachynski, A. V.; Kuzmin, A. N.; Nyk, M.; Roy, I.; Prasad, P. N. Zinc Oxide Nanocrystals for Nonresonant Nonlinear Optical Microscopy in Biology and Medicine. *J. Phys. Chem. C* **2008**, *112*, 10721–10724.
14. Ohulchanskyy, T. Y.; Roy, I.; Yong, K. T.; Pudavar, H. E.; Prasad, P. N. High-Resolution Light Microscopy Using Luminescent Nanoparticles. *Wiley Interdiscip. Rev. Nanomed. Nanobiotechnol.* **2010**, *2*, 162–175.
15. Wang, F.; Deng, R. R.; Wang, J.; Wang, Q. X.; Han, Y.; Zhu, H. M.; Chen, X. Y.; Liu, X. G. Tuning Upconversion through Energy Migration in Core-Shell Nanoparticles. *Nat. Mater.* **2011**, *10*, 968–973.
16. Wang, F.; Banerjee, D.; Liu, Y. S.; Chen, X. Y.; Liu, X. G. Upconversion Nanoparticles in Biological Labeling, Imaging, and Therapy. *Analyst* **2010**, *135*, 1839–1854.
17. Mader, H. S.; Kele, P.; Saleh, S. M.; Wolfbeis, O. S. Upconverting Luminescent Nanoparticles for Use in Bioconjugation and Bioimaging. *Curr. Opin. Chem. Biol.* **2010**, *14*, 582–596.
18. Chatterjee, D. K.; Gnanasammandhan, M. K.; Zhang, Y. Small Upconverting Fluorescent Nanoparticles for Biomedical Applications. *Small* **2010**, *6*, 2781–2795.

19. Zhou, J.; Liu, Z.; Li, F. Y. Upconversion Nanophosphors for Small-Animal Imaging. *Chem. Soc. Rev.* **2012**, *41*, 1323–1349.
20. Shen, J.; Zhao, L.; Han, G. Lanthanide-Doped Upconverting Luminescent Nanoparticle Platforms for Optical Imaging-Guided Drug Delivery and Therapy. *Adv. Drug Delivery Rev.* **2012**, 10.1016/j.addr.2012.05.007.
21. Bogdan, N.; Vetrone, F.; Ozin, G. A.; Capobianco, J. A. Synthesis of Ligand-Free Colloidally Stable Water Dispersible Brightly Luminescent Lanthanide-Doped Upconverting Nanoparticles. *Nano Lett.* **2011**, *11*, 835–840.
22. Haase, M.; Schäfer, H. Upconverting Nanoparticles. *Angew. Chem., Int. Ed.* **2011**, *50*, 5808–5829.
23. Heer, S.; Kömpe, K.; Güdel, H. U.; Haase, M. Highly Efficient Multicolour Upconversion Emission in Transparent Colloids of Lanthanide-Doped $NaYF_4$ Nanocrystals. *Adv. Mater.* **2004**, *16*, 2102–2105.
24. Chatteriee, D. K.; Rufalhah, A. J.; Zhang, Y. Upconversion Fluorescence Imaging of Cells and Small Animals Using Lanthanide Doped Nanocrystals. *Biomaterials* **2008**, *29*, 937–943.
25. Wu, S. W.; Han, G.; Milliron, D. J.; Aloni, S.; Altoe, V.; Talapin, D. V.; Cohen, B. E.; Schuck, P. J. Non-Blinking and Photostable Upconverted Luminescence from Single Lanthanide-Doped Nanocrystals. *Proc. Natl. Acad. Sci. U. S. A.* **2009**, *106*, 10917–10921.
26. Nam, S. H.; Bae, Y. M.; Park, Y. I.; Kim, J. H.; Kim, H. M.; Choi, J. S.; Lee, K. T.; Hyeon, T.; Suh, Y. D. Long-Term Real-Time Tracking of Lanthanide Ion Doped Upconverting Nanoparticles in Living Cells. *Angew. Chem., Int. Ed.* **2011**, *50*, 6093–6097.
27. Chen, G. Y.; Ohulchanskyy, T. Y.; Kachynski, A.; Ågren, H.; Prasad, P. N. Intense Visible and Near-Infrared Upconversion Photoluminescence in Colloidal $LiYF_4:Er^{3+}$ Nanocrystals under Excitation at 1490 nm. *ACS Nano* **2011**, *5*, 4981–4986.
28. Xu, C. T.; Svenmarker, P.; Liu, H. C.; Wu, X.; Messing, M. E.; Wallenberg, L. R.; Andersson-Engels, S. High-Resolution Fluorescence Diffuse Optical Tomography Developed with Nonlinear Upconverting Nanoparticles. *ACS Nano* **2012**, *6*, 4788–4795.
29. Liu, Q.; Sun, Y.; Yang, T. S.; Feng, W.; Li, C. G.; Li, F. Y. Sub-10 nm Hexagonal Lanthanide-Doped $NaLuF_4$ Upconversion Nanocrystals for Sensitive Bioimaging *in Vivo*. *J. Am. Chem. Soc.* **2011**, *133*, 17122–17125.
30. Xiong, L. Q.; Chen, Z. G.; Tian, Q. W.; Cao, T. Y.; Xu, C. J.; Li, F. Y. High Contrast Upconversion Luminescence Targeted Imaging *in Vivo* Using Peptide-Labeled Nanophosphors. *Anal. Chem.* **2009**, *81*, 8687–8694.
31. Nyk, M.; Kumar, R.; Ohulchanskyy, T. Y.; Bergey, E. J.; Prasad, P. N. High Contrast *in Vitro* and *in Vivo* Photoluminescence Bioimaging Using Near Infrared to Near Infrared Up-Conversion in Tm^{3+} and Yb^{3+} Doped Fluoride Nanophosphors. *Nano Lett.* **2008**, *8*, 3834–3838.
32. Zhang, F.; Braun, G. B.; Shi, Y. F.; Zhang, Y. C.; Sun, X. H.; Reich, N. O.; Zhao, D. Y.; Stucky, G. Fabrication of $Ag@SiO_2@Y_2O_3:Er$ Nanostructures for Bioimaging: Tuning of the Upconversion Fluorescence with Silver Nanoparticles. *J. Am. Chem. Soc.* **2010**, *132*, 2850–2851.
33. Zhang, H.; Li, Y. J.; Ivanov, I. A.; Qu, Y. Q.; Huang, Y.; Duan, X. F. Plasmonic Modulation of The Upconversion Fluorescence in $NaYF_4$:Yb/Tm Hexaplate Nanocrystals Using Gold Nanoparticles or Nanoshells. *Angew. Chem., Int. Ed.* **2010**, *49*, 2865–2868.
34. Yi, G. S.; Chow, G. M. Water-Soluble $NaYF_4$:Yb,Er(Tm)/$NaYF_4$/Polymer Core/Shell/Shell Nanoparticles with Significant Enhancement of Upconversion Fluorescence. *Chem. Mater.* **2007**, *19*, 341–343.
35. Chen, G. Y.; Ohulchanskyy, T. Y.; Law, W. C.; Ågren, H.; Prasad, P. N. Monodisperse $NaYbF_4:Tm^{3+}/NaGdF_4$ Core/Shell Nanocrystals with Near-Infrared to Near-Infrared Upconversion Photoluminescence and Magnetic Resonance Properties. *Nanoscale* **2011**, *3*, 2003–2008.
36. Chen, G. Y.; Ohulchanskyy, T. Y.; Kumar, R.; Ågren, H.; Prasad, P. N. Ultrasmall Monodisperse $NaYF_4:Yb^{3+}/Tm^{3+}$ Nanocrystals with Enhanced Near-Infrared to Near-Infrared Upconversion Photoluminescence. *ACS Nano* **2010**, *4*, 3163–3168.
37. Wang, G. F.; Peng, Q.; Li, Y. D. Upconversion Luminescence of Monodisperse $CaF_2:Yb^{3+}/Er^{3+}$ Nanocrystals. *J. Am. Chem. Soc.* **2009**, *131*, 14200–14201.
38. Wang, Y. F.; Sun, L. D.; Xiao, J. W.; Feng, W.; Zhou, J. C.; Shen, J.; Yan, C. H. Rare-Earth Nanoparticles with Enhanced Upconversion Emission and Suppressed Rare-Earth-Ion Leakage. *Chem.—Eur. J.* **2012**, *18*, 5558–5564.
39. Dong, N. N.; Pedroni, M.; Piccinelli, F.; Conti, G.; Sbarbati, A.; Ramírez-Hernández, J. E.; Maestro, L. M.; Iglesias-de la Cruz, M. C.; Sanz-Rodriguez, F.; Juarranz, A.; *et al*. NIR-to-NIR Two-Photon Excited $CaF_2:Tm^{3+},Yb^{3+}$ Nanoparticles: Multifunctional Nanoprobes for Highly Penetrating Fluorescence Bio-Imaging. *ACS Nano* **2011**, *5*, 8665–8671.
40. Liu, R.; Tu, D. T.; Liu, Y. S.; Zhu, H. M.; Li, R. F.; Zheng, W.; Ma, E.; Chen, X. Y. Controlled Synthesis and Optical Spectroscopy of Lanthanide-Doped $KLaF_4$ Nanocrystals. *Nanoscale* **2012**, *4*, 4485–4491.
41. Shan, J. N.; Uddi, M.; Yao, N.; Ju, Y. G. Anomalous Raman Scattering of Colloidal Yb^{3+},Er^{3+} Codoped $NaYF_4$ Nanophosphors and Dynamic Probing of the Upconversion Luminescence. *Adv. Funct. Mater.* **2010**, *20*, 3530–3537.
42. Krämer, K. W.; Biner, D.; Frei, G.; Güdel, H. U.; Hehlen, M. P.; Lüthi, S. R. Hexagonal Sodium Yttrium Fluoride Based Green and Blue Emitting Upconversion Phosphors. *Chem. Mater.* **2004**, *16*, 1244–1251.
43. Boyer, J. C.; van Veggel, F. C. J. M. Absolute Quantum Yield Measurements of Colloidal $NaYF_4:Er^{3+}, Yb^{3+}$ Upconverting Nanoparticles. *Nanoscale* **2010**, *2*, 1417–1419.
44. Filion, T. M.; Kutikov, A.; Song, J. Chemically Modified Cellulose Fibrous Meshes for Use as Tissue Engineering Scaffolds. *Bioorg. Med. Chem. Lett.* **2011**, *21*, 5067–5070.
45. Zhang, T. R.; Ge, J. P.; Hu, Y. P.; Yin, Y. D. A General Approach for Transferring Hydrophobic Nanocrystals into Water. *Nano Lett.* **2007**, *7*, 3203–3207.
46. Schneider, G.; Decher, G. Functional Core/Shell Nanoparticles *via* Layer-by-Layer Assembly. Iinvestigation of the Experimental Parameters for Controlling Particle Aggregation and for Enhancing Dispersion Stability. *Langmuir* **2008**, *24*, 1778–1789.